JOURNAL OF COMPUTATIONAL PHYSICS 104, 287–302 (1993)

A Comparison of the Contour Surgery and Pseudo-spectral Methods

BERNARD LEGRAS

Laboratoire de Météorologie Dynamique du CNRS, École Normale Supérieure, 24 rue Lhomond, 75231 Paris Cedex 05, France

AND

DAVID G. DRITSCHEL

Department of Applied Mathematics and Theoretical Physics, University of Cambridge, Silver Street, Cambridge CB3 9EW, United Kingdom

Received May 21, 1991; revised April 7, 1992

Two very different numerical methods which have been used to simulate high Reynolds number two-dimensional flows are compared for the first time. One method, the pseudo-spectral method, is fundamentally based on the Eulerian description of fluid flow and the other, the contour surgery method, is inherently Lagrangian. The former makes use of a continuous distribution of vorticity, while the latter, a theoretically inviscid method, makes use of a discrete distribution. A comparison is nevertheless attempted in a model problem wherein the initial vorticity distribution is continuous. We examine the stripping of an initially circular vortex by applied adverse shear in doubly periodic geometry. The constraining geometry causes the flow to become very complex, placing great demands on both computational methods. The surprise is that as few as eight discrete levels of vorticity in contour surgery give results which are quantitatively close to those obtained by the pseudo-spectral method at high resolution. Advantages and shortcomings of both methods are noted.

1. INTRODUCTION

Experiments in computational fluid dynamics are playing a central role in understanding two-dimensional flows. Such flows are idealizations of numerous practical situations, particularly geophysical ones, owing to stratification and rotation-induced strong layerwise two-dimensionality. However, these flows are difficult to examine in a clean laboratory experiment, whereas they are becoming increasingly easy to generate on a computer. In addition, the power of modern scientific computers enables one to address questions related to the dynamics of small-scale structures by unobtrusively probing the flow at a high density of points and at a high frequency, something virtually impossible at present in laboratory experiments.

There exists a great variety of numerical algorithms which have been developed for the numerical simulation of two-dimensional flows. In theoretical studies of high Reynolds number (inertial) flows, though, where the fluid is not constrained by complicated boundaries, this variety is considerably smaller.

The most popular algorithm is certainly the *pseudo-spectral method* [1] which is suited for periodic geometry or simple boxes. In this method, the variables of the flow (vorticity, velocity) in the physical domain are represented as complex coefficients in a dual spectral domain for which a convenient basis is provided by the family of eigenmodes of the Laplace operator (the Fourier basis in a doubly periodic plane). The spatial derivatives can be estimated with high accuracy by simple multiplications of the spectral coefficients, and the solution of the Poisson problem is elementary. The calculation of the nonlinear advective terms which would lead to convolutions in the spectral domain is performed in the physical domain, again by simple multiplications. The overall speed of the algorithm relies on the existence or nonexistence of fast transforms between the physical and the spectral domains. The algorithm is thus much more efficient in doubly periodic planar geometry, where fast Fourier transforms are available than, say, in spherical geometry for which there exist only half-fast transforms.

A major feature of this method, the fact that it provides a uniform spatial resolution at the scale of the smallest resolved structure, turns out also to be its major limitation. In practical circumstances, where small scales are generated within a very small portion of the physical domain, a considerable waste of computer time occurs since the algorithm spends the same amount of time computing fluid motions in all parts of the domain. Also, there is no consideration given to the considerable time-variability of the flow complexity—a very quiescent flow should require less computation than a very agitated one. The source of this faulty behavior is that the algorithm is based on an Eulerian representation and thus does not explicitly incorporate the

0021-9991/93 $5.00

fundamental property of vorticity conservation on fluid particles.

An early attempt to provide a Lagrangian formulation was the *vortex method*. In this method, the flow (the vorticity distribution) is represented by a cloud of point vortices. It has been applied to a number of situations with localized structures and seems particularly suited for the dynamics of vortex sheets. Details of this method and its applications may be found in the review by Leonard [2].

A more recent method, originally proposed by Zabusky *et al.* [3], is *contour dynamics*, a method based on the observation that the evolution of a patch of uniform vorticity is fully described by the evolution of its bounding contour. In principle, contour dynamics thereby reduces a two-dimensional problem to a one-dimensional problem. The velocity anywhere in the fluid, particularly on the contours, where it is needed for the contour's evolution, is determined by inversion, using Green's function of the associated Laplace operator. The method is not limited to a patch of uniform vorticity: several contours can be nested in a stack, thus providing an approximation of distributed vortices.

Typically, the contours of vorticity patches generate very intricate small-scale structures through the nonlinear cascade mechanism of filamentation [4, 5]. The method is able to cope with this problem by a series of subsidiary algorithms handling the parameterization of the contours and the removal of sufficiently fine-scale filamentary structures. The most advanced version of contour dynamics, known as *contour surgery*, is fully documented in [5].

The validity of this method has, however, often been questioned up to very recently. A common criticism is that the dynamics of uniform patches with their discontinuous distribution of vorticity could produce artifacts which are irrelevant to the dynamics of distributed vortices. It has even been argued [10] that contour dynamics could produce spurious singularities. This latter charge has been cleared completely in [11, 12], and the regularity of contour dynamics has received a mathematical proof in [18]. There has remained, however, the question of just how well a continuous distribution of vorticity can be modelled using discrete vorticity jumps in contour surgery. The only convincing way to answer this question, it seemed to us, was by performing a direct comparison between contour surgery and the pseudo-spectral method, the results of which are reported here.

This comparison is based on one selected case which is the stripping of an initially circular vortex by an external shear flow in doubly periodic planar geometry. This geometry is ideal for the pseudo-spectral method, though it is significantly less convenient for the contour surgery method and some adaptation of the existing contour surgery method has been necessary. Additionally, for the initialization of the contour surgery calculations, it is necessary to discretize the continuous vorticity profile of the starting vortex (8 and 16 discrete levels are used here). The resolution used in the pseudo-spectral experiments is high enough to resolve many of the filamentary structures which are typical of contour dynamics experiments. The duration of the temporal integration is also long enough to allow very complicated dynamics to occur.

In Section 2, we present the numerical algorithms used in this study and the initial conditions for the investigated case. We describe, in particular, the procedure for the discretization of continuous vorticity profiles used to initialize the contour surgery experiments. In Section 3, we present a movie of the temporal development. Section 4 contains the central results of this article. Here we show the remarkably close agreement obtained between the results calculated by the two methods. Enlargements of details are necessary to analyze slight discrepancies. Further discussion and some concluding remarks are offered in Section 5.

2. DESCRIPTION OF THE EXPERIMENTS

2.1. *The Test Problem*

The experiments are conducted in a hypothetical two-dimensional, incompressible fluid in the nearly invisid limit. For this fluid, vorticity is a natural variable owing to its material conservation in the absence of dissipation. Both numerical models simulate the vorticity equation

$$\frac{\partial \omega}{\partial t} + J(\psi, \omega) + U\frac{\partial \omega}{\partial x} = D(\omega) \tag{1}$$

in a doubly periodic box $[-\pi, \pi] \times [-\pi, \pi]$. Here, $\omega = \Delta\psi$, ψ is the streamfunction, $U(y)$ is an imposed, external mean flow, and $D(\omega)$ is a dissipation operator (described later in this section).

A single, initially circular vortex is subjected to adverse shear, $U = 2\pi\Lambda y$, with the dimensionless shear Λ chosen to produce severe stripping of the peripheral vorticity layers ($\Lambda = 0.11$). The initial radial vorticity profile, Fig. 1, is given by

$$\omega(r) = \begin{cases} \pi(1 + \cos \pi r), & \text{if } 0 \leqslant r \leqslant 1, \\ 0, & \text{if } r > 1, \end{cases} \tag{2}$$

corresponding to a broadly distributed initial distribution of vorticity. Such distributions are particularly sensitive to the effects of shear [13]. One may note that the imposed shear has, in fact, infinite vorticity at the periodic boundary $y = -\pi$ and $y = \pi$. This vortex sheet, however, has no impact on the dynamics inside the domain since it is fixed in position and, in practice, no part of the interior vortex reaches this periodic interface. In the pseudo-spectral code, the sheet is spread out over a thin layer of width $0.05(2\pi)$, where the shear is $\Lambda = -2.09$. Numerical stability is

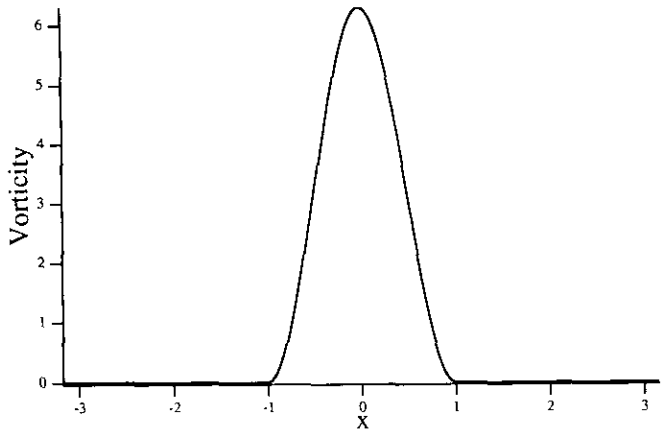

FIG. 1. The initial radial vorticity profile used in the experiment.

obtained by filtering out the vorticity within this region. The value of the internal shear Λ is just under the critical value $\Lambda_c \approx 0.115$, above which the vortex is torn apart.

2.2. *Simulation by Pseudo-Spectral Method*

We are not going to review here the pseudo-spectral method beyond the general ideas given in Section 1. The reader is referred to [1] for a comprehensive discussion. Our scope is only to cover the relevant features pertaining to our calculations.

The method used here calculates the Jacobian in *physical* space as

$$J(\psi, \omega) = \frac{\partial \psi}{\partial x}\frac{\partial \omega}{\partial y} - \frac{\partial \psi}{\partial y}\frac{\partial \omega}{\partial x},$$

where the spatial derivatives are calculated in *spectral* space. There exist formulations of the Jacobian leading to faster calculations, [14], but we can here directly incorporate the mean flow without any Gibbs effects by adding $U(y)$ to $-\partial\psi/\partial y$.

Since the investigated case exhibits a symmetry with respect to the center of the domain, all the Fourier coefficients for vorticity and streamfunction are real and those for the velocity components are pure imaginary. Taking into account this property, an appropriate recombination of the Fourier transforms allows one to reduce the amount of computation by about a factor of two.

The resolution used is 1024×1024 in the physical domain. The spectral representation is truncated within a circular domain in the Fourier plane, that is, all the Fourier modes with wavenumbers $|k^2 + l^2|^{1/2} > 507$ are discarded. This truncation tries to preserve isotropy in spite of the basic squared periodicity. It also induces a partial de-aliasing of the nonlinear terms. Full de-aliasing is not performed because it was found that, using a physical grid of 512×512, the correction then introduced was of the order of the truncation error of the computer. This is a fortiori true here.

Dissipation of enstrophy is performed by the hyperviscosity operator

$$D(\omega) = -\nu_8 \Delta^4 \omega$$

with $\nu_8 = 4.6 \times 10^{-20}$. Similar parameterizations of dissipation and subgrid turbulence are widely used in two-dimensional computational fluid dynamics. They aim at dissipating the enstrophy at the end of its nonlinear cascade to small scales, providing a well, into which the cascaded enstrophy is lost. While a better parameterization of the unresolved enstrophy cascade may be possible [15], this dissipation process is easy to implement, computationally inexpensive, and very selective, requiring one to devote only a small spectral range to dissipation. Although the harmlessness of this approximation to the physics has yet to be proven rigorously, there exists no clear counter indication as far as the flow is essentially inertial. It can be argued that there are no viscously driven instabilities in two dimensions that would be sensitive to such a parameterization. The flow is indeed governed by the energy-containing large-scale motions. A conservative standpoint is to say that the spurious effects of hyperviscosity, if any, should be contained within the portion of energy dissipated. We will see that this effect is negligible for the resolution used here.

Time-stepping is done with an Adams–Bashforth scheme with an explicit treatment of the linear dissipative term. For a variable $z(t)$ governed by the equation

$$\frac{dz(t)}{dt} = F(t) - \nu z(t),$$

where F is an arbitrary nonlinear operator depending on $z(t)$ and other variables and ν is a fixed damping coefficient, the Adams–Bashforth scheme is

$$z(t + \Delta t) = e^{-\nu \Delta t}\left(z(t) + \frac{\Delta t}{2}\left(3F(t) - e^{-\nu \Delta t}F(t - \Delta t)\right)\right). \tag{3}$$

This scheme is readily applied to the evolution equation of Fourier coefficients derived from Eq. (1). The first step is done using a half Euler step and a half leapfrog step. The Adams–Bashforth scheme is second-order in time and shows remarkable stability properties. It does not produce any spurious numerical oscillations like the leapfrog scheme and thus does not require a corrective step during the temporal integration. The time step is $\Delta t = 5 \times 10^{-4}$ for the experiment described below.

The CPU cost of the code, including diagnostics not presented here, is 1.1 s per time step using one processor on a Cray 2. The experiment required 50,000 time steps.

2.3. *Simulation by Contour Surgery*

The basic ideas behind contour dynamics and its extension to surgery are reviewed in [5]. Here, we review only the basic definitions of the numerical parameters then pass to two new considerations: (1) the extension of the algorithm to doubly periodic geometry; and (2) the optimal discretization of a continuous vorticity distribution into a finite number of uniform vorticity regions.

The operation of the contour surgery algorithm is governed by three principal parameters: the time step Δt, the typical distance between adjacent nodes comprising a contour μ, and the scale at which filamentary vorticity is removed δ. Unlike the pseudo-spectral method, this Lagrangian method has no analogous CFL criterion. What governs accuracy is the maximum rate of stretching or twisting [11] along a contour; experience indicates that this is typically comparable to or less than the peak vorticity magnitude in the flow [5, 11]. For peak vorticity 2π, the recommended time step is $\Delta t = 0.05$, and this is used here. Note that the time step is one hundred times larger than that used in the pseudo-spectral experiment.

The node spacing is variable in time and is proportional to μ and inversely proportional to the two-thirds power of a weighted sum of nearby curvature values. This relationship was chosen to link consistently with surgical dissipation at the scale $\delta = \frac{1}{8}\mu^2 L$, where L is a fixed parameter setting the overall size of the vorticity distribution (here, $L = 1$, the initial vortex radius). Surgery *selectively* removes small-scale features: thin filamentary structures are removed while sharp vorticity edge gradients are not. This has important ramifications in the comparisons presented below.

The doubly periodic algorithm is obtained from the singly periodic one (described in [5]) by periodically extending and then summing the singly periodic Green function, taking into account the requirement that the total circulation must vanish in any basic box. The singly periodic Green function is

$$G_s(x, y) = (4\pi)^{-1} \log[\cosh(y) - \cos(x)], \tag{4}$$

where x and y here stand for the coordinate differences between the source and the evaluation points. We construct the doubly periodic Green function from

$$\begin{aligned} G_d(x, y) = {} & G_R(x, y) + G_s(x, y) \\ & + \sum_{n=1}^{\infty} \{G_s(x, y + 2\pi n) - G_s(0, 2\pi n) \\ & + G_s(x, y - 2\pi n) - G_s(0, -2\pi n)\}, \end{aligned} \tag{5}$$

where G_R is a regular (non-singular) function chosen to ensure zero total circulation in each $2\pi \times 2\pi$ box. It satisfies $\nabla^2 G_R = C$ for some constant C (G_R corresponds to uniform vorticity within the box). Since the rest of G_d is periodic in x, though not in y, G_R must depend on y alone, and hence the only form it can take is $G_R = \frac{1}{2}Cy^2$. The constant C is determined from the constraint of zero total circulation—the area integral of $\nabla^2 G_d$ over any box must vanish. We find that C is just the negative of the inverse area of the box, $C = -1/4\pi^2$.

A closed form expression for the sum over G_s in the expression for G_d is not known, but in practice it is sufficient to take just the first two terms in the sum. The first neglected term is then $O(e^{-5\pi}) \approx O(10^{-7})$. More directly, a test calculation using the first three terms could not be distinguished from a calculation using two.

The second new feature is the method for approximating a given continuous distribution of vorticity by a finite number of nested, uniform regions of vorticity. The method seeks the discrete distribution of vorticity which is closest to a given continuous distribution in a least-squares sense, subject to the constraint that the total circulation of the two distributions is the same. In other words, the object is to find the areas A_j and uniform vorticities ω_j of a superposition of N disks which minimize the function

$$\begin{aligned} & F(A_1, \ldots, A_N, \omega_1, \ldots, \omega_N) \\ & \quad \equiv \int_0^{A_{\max}} [\omega(A) - \bar{\omega}(A)]^2 \, dA, \end{aligned} \tag{6}$$

subject to the constraint

$$\begin{aligned} & G(A_1, \ldots, A_N, \omega_1, \ldots, \omega_N) \\ & \quad \equiv \int_0^{A_{\max}} [\omega(A) - \bar{\omega}(A)] \, dA = 0, \end{aligned} \tag{7}$$

where $\omega(A)$ is the given continuous distribution as a function of area ($= \pi r^2$ here) and $\bar{\omega}(A)$ is the unknown discrete distribution (see Fig. 2). In general, the contour locations lie along certain contours of constant vorticity within the continuous distribution. These contours are simply circles for the initial conditions considered in this paper. In any case, the formal solution to the above optimization problem is obtained by solving the following nonlinear tridiagonal equation for the contour areas A_j:

$$\begin{aligned} \omega(A_j) = {} & \frac{1}{A_j - A_{j-1}} \int_{A_{j-1}}^{A_j} \omega(A) \, dA \\ & + \frac{1}{A_{j+1} - A_j} \int_{A_j}^{A_{j+1}} \omega(A) \, dA, \end{aligned} \tag{8}$$

subject to the boundary conditions $A_0 = 0$ and

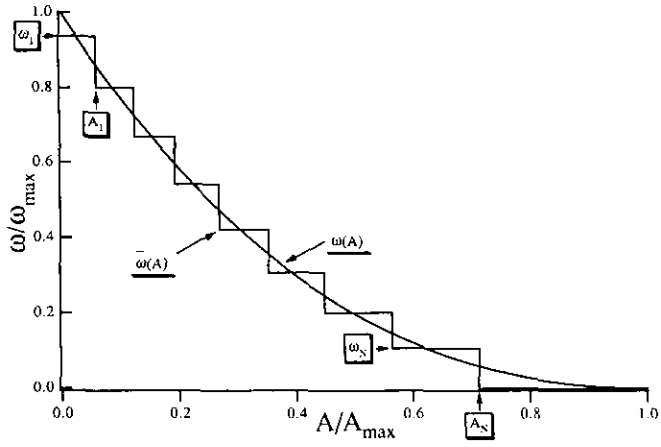

FIG. 2. The discrete profile used in the contour surgery experiment compared to the continuous profile.

$A_{N+1} = A_{\max}$. After obtaining the A_j (using a shooting method), the ω_j are obtained from

$$\omega_j = \frac{1}{A_j - A_{j-1}} \int_{A_{j-1}}^{A_j} \omega(s)\, dA + C, \tag{9}$$

where

$$C = \frac{1}{A_N} \int_{A_N}^{A_{\max}} \omega(A)\, dA. \tag{10}$$

Table I gives the eight- and 16-disk discretization of the continuous profile used in this paper.

The initial spatial resolution used in the contour surgery calculations was $\mu = 0.06$, corresponding to approximately 105 nodes around a circular contour of unit radius. The resolution adjusts to the complexity of the flow so that, in the calculations presented here, the total number of nodes increases 20-fold. Correspondingly, the computational cost increases 400-fold. After time $t = 20.5$ in the eight-contour calculation, μ was increased to 0.09 to ease the computational cost, and after time $t = 14.5$ in the 16-contour calculation, μ was increased to 0.07. Each calculation required several days of CPU time on a single processor of a Cray-XMP, the cost being so great, due to the inefficiency of computing in doubly periodic geometry. In infinite geometry, the cost would be reduced by a factor of approximately four (less than a day of CPU would then be required). The cost (in seconds) per time step in this case is 4.0×10^{-6} times the total number of nodes squared. For instance, one time step for 10,000 nodes takes 400 s. Taking into account the faster processor speed of the Cray-2 used for the pseudo-spectral calculation and the exploitation of symmetry therein, both methods required nearly the same computational resources in this example.

TABLE I

Vorticity Levels for an Optimally Discretized Cosine Vorticity Profile and the Corresponding Vorticity Values in the Continuous Profile

8 levels			16 levels		
r_j	ω_j	$\omega(r_j)$	r_j	ω_j	$\omega(r_j)$
0.24362437	0.93678869	0.86056355	0.17537481	0.96487331	0.92601217
0.35075009	0.79966629	0.72594480	0.25021921	0.89151572	0.85330983
0.43813176	0.66755120	0.59657167	0.30930349	0.81946864	0.78194590
0.51720127	0.54092003	0.47299345	0.36063998	0.74878786	0.71197962
0.59302441	0.42039477	0.35594872	0.40735672	0.67953607	0.64347788
0.66924549	0.30683055	0.24650015	0.45109561	0.61178439	0.57651699
0.75008265	0.20149763	0.14635482	0.49287885	0.54561428	0.51118494
0.84391119	0.10653989	0.05892007	0.53343004	0.48112030	0.44758469
			0.57332412	0.41841378	0.38583865
			0.61307427	0.35762822	0.32609544
			0.65319810	0.29892736	0.26854025
			0.69428897	0.24251784	0.21341187
			0.73712446	0.18867060	0.16103303
			0.78288466	0.13776016	0.11187093
			0.83372287	0.09034640	0.06668168
			0.89493707	0.04738165	0.02698935

Note. r_j is the radius of the jth jump in vorticity in the discrete profile (i.e., $r_j = (A_j/\pi)^{1/2}$), ω_j is the vorticity just inside r_j, and $\omega(r_j)$ is the vorticity of the corresponding continuous profile at $r = r_j$.

3. THE EXPERIMENT

This section presents a movie of the flow evolution computed by the pseudo-spectral method. Figure 3 shows a series of vorticity charts extracted from the experiment. The charts are not regularly spaced in time but show the most interesting stages of the experiment. The first four are full views of the periodic box while the other ones are enlargements of the central region (with scale $\frac{11}{16}$). The plotted contours are the vorticity levels corresponding to the steps of the eight-level discretization used in the contour surgery experiment (see Table I).

The initial circular shape, Fig. 3a, is rapidly deformed by the shear and wide arms are expelled on both sides of the vortex at $t = 4$, Fig. 3b. In an unbounded domain, the expelled vorticity would be pulled away toward infinity, but here, in a periodic plane, it re-enters across the lateral boundaries as seen at $t = 7$, Fig. 3c. A practical situation corresponding to this flow is a row of vortices injected in a shear layer. One also sees that the arms reduce to thin filaments except near their extremity and that the core of the vortex tends to align its major axis perpendicular to the direction of the shear, or at a 45° angle with respect to the background strain axes. At $t = 10$, Fig. 3d, the re-entering filament has passed by the vortex and is continuing its way toward a second turn. The expelled filament is now

connected to the vortex by a very small section. It can be shown that at this stage there exists an approximate functional relationship between the vorticity and the total streamfunction inside the stripped vortex core so that $J(\psi - \frac{1}{2}Ay^2, \omega) \approx 0$. In other words, the vortex is nearly in equilibrium with the shear. Another interesting feature is that the stripping of the external vorticity layers produces an exceedingly sharp vorticity gradient at the frontier of the vortex (this effect is even more pronounced in the corresponding contour surgery experiment which we will come to in Section 4).

As time proceeds further, the flow becomes more complicated, though more interesting for our purpose. The complication arises from the interaction of the re-entering filaments with the vortex core. In the quasi-stationary situation of Fig. 3d, the small domain near the connection of the filament to the vortex contains a stagnation point in the total velocity field, corresponding to a separatrix crossing in the streamfunction field. In infinite geometry, this stagnation point has little consequence for the ensuing dynamics, but here it causes a complicated interaction between the re-entering filament and the vortex core. This filament, being divided by one of the separatrices stemming from the stagnation point, splits into two parts near the stagnation point. One part is cast away to begin a new turn, and another part is advected along and brought very close to the flank of the vortex. This phenomenon is clearly visible at $t = 13$, Fig. 3e, where one sees also the strong perturbation induced on the vortex itself.

The next stages of the evolution, Figs. 3f and g, at $t = 15.5$ and $t = 17.5$, involve further splitting and folding of the filaments around the vortex. The mixing of vorticity produced here is by no means a down-gradient process, but falls within the category of Hamiltonian chaos studied by

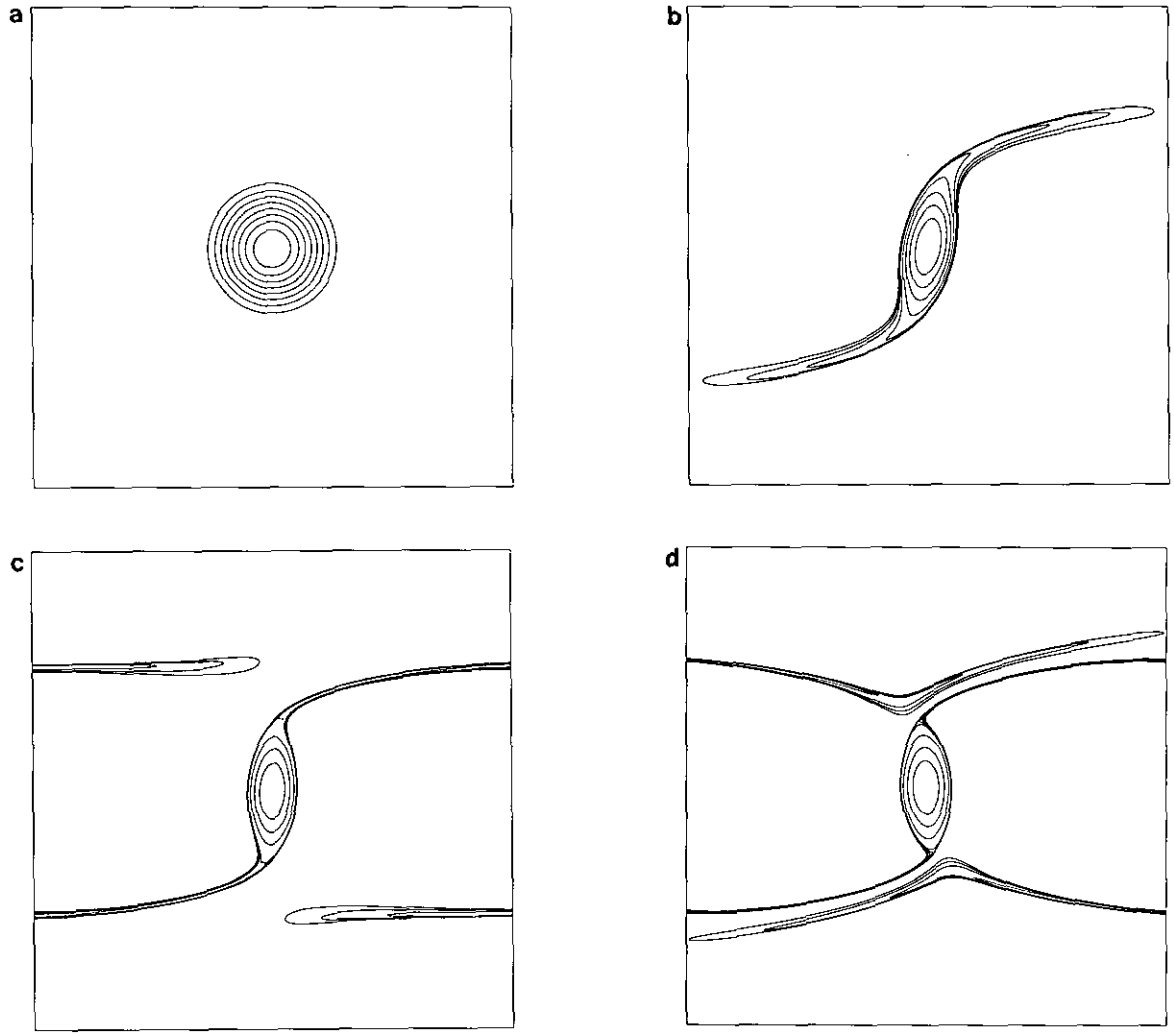

FIG. 3. Vorticity charts taken from the pseudo-spectral experiment. The plotted contours are those used in the contour surgery experiment with eight levels. The frame of the charts is the full periodic box for (a) to (d) and the domain $[-0.6\pi, 0.6\pi] \times [-0.6\pi, 0.6\pi]$ for the other cases: (a) $t = 0$; (b) $t = 4$; (c) $t = 7$; (d) $t = 10$; (e) $t = 13$; (f) $t = 15.5$; (g) $t = 17.5$; (h) $t = 21$; (i) $t = 23.5$; (j) $t = 25$.

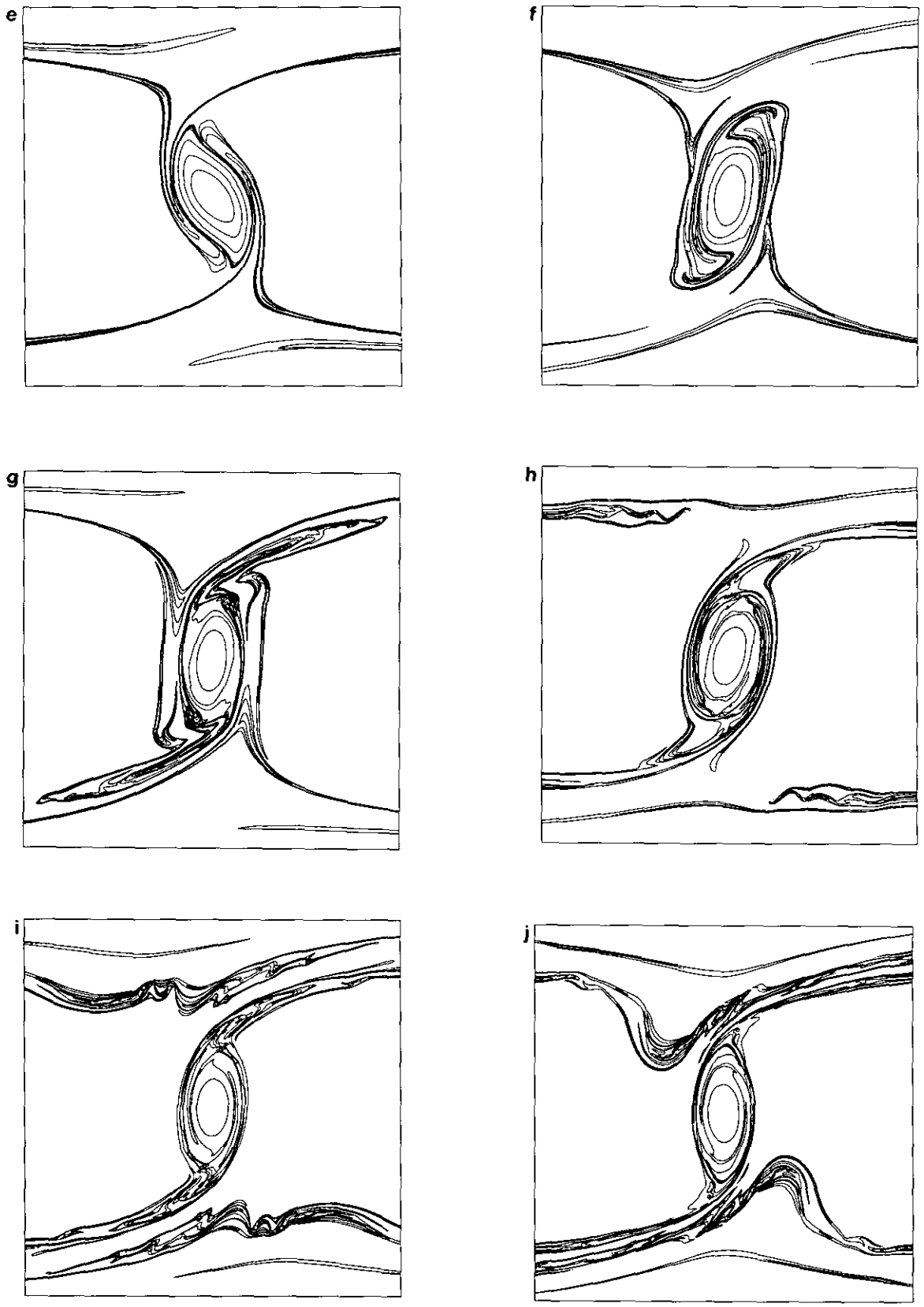

FIG. 3—*Continued*

Ottino and collaborators [16]. Since dissipation acts only at very small scales, the flow contains a large amount of detail within the magma of filaments accumulated around the vortex. There is little need to point out that this situation is not a trivial basis for our comparison.

As long as the re-entering filaments stay a distance from the vortex, their effect on the vortex is very limited. This was the case during the initial stages of the experiment, $t \leqslant 11$, and becomes true again around $t = 20$. Consequently, the vortex core, at $t = 21$ and $t = 23.5$, Figs. 3h and i is much closer in shape to an ellipse than at the previous stage of the experiment. From $t = 20$ to $t = 23.5$, the filaments are wrapped around the core and are stripped away by the external shear, much in the same way that the weak external levels were originally removed. The shape of the core at $t = 23.5$ is, in fact, very reminiscent of the shape at $t = 10$ (see Fig. 3d), near the end of the initial stage of the evolution, in which one sees a quasi-elliptical core lying perpendicular to the direction of the shear. It is again possible to find a functional relationship between the vorticity and the streamfunction, though in a smaller region than at $t = 10$. The less intricate structure of the filaments around the core at $t = 23.5$ than at $t = 21$ is due to dissipation and smoothing of the vorticity profile by the hyperviscosity arising from the acute thinning of filaments spun around the vortex core.

The wavy structure of the re-entering filaments is not due to a kind of Kelvin–Helmholtz instability but is the trace of their partial folding upon passing near the stagnation point at an earlier time. This mechanism is well illustrated in Figs. 3f and g.

At $t = 25$, Fig. 3j, which is the final time of the experiment displayed here, a new phase of strong interaction between re-entering filaments and the vortex core begins, during which the vortex again experiences major deformations from an elliptical shape.

As regards to numerical accuracy, the total enstrophy loss is 9% of its initial value, while the total energy is conserved up to the fifth digit. The dissipation is, however, sufficient to provide a clear small-scale cutoff in the energy spectrum during the whole duration of the experiment, without any spurious tendency to accumulate enstrophy near the truncation scale. The evolution is thus basically inertial, though the finite resolution and hyperviscosity have stopped vorticity gradient intensification well short of that observed in the corresponding contour surgery calculations described below. We will discuss the consequences of this in the following sections.

4. COMPARISON WITH CONTOUR SURGERY

4.1. *Early Time Comparison*

Figures 4a–f show six charts taken from the contour surgery experiment with the eight-contour discretization at $t = 10$, 15.5, 17.5, 21, 23.5, and 25. They must be compared with Figs. 3d and 3f–j. There is clear evidence that the agreement between the two methods is excellent. The structure of the vorticity field, up to the location of very small-scale details, is practically the same with both methods at all the stages of the evolution. If the corresponding charts for both methods could be superimposed, as is possible on a viewgraph, the contours would be seen to coincide to a very good approximation up to $t = 12$ and to stay very close for the sequel of the evolution, except for some details at the very latest times. There is no trace of any spurious singular behavior in contour surgery that would affect the largest scales of the flow. This agreement is all the more remarkable as the problems studied are not really identical: the continuous profile of vorticity is resolved to a very high accuracy in the pseudo-spectral method while it is resolved by only a few large steps in contour surgery. This in turn enables contour surgery much more resolution of filaments without being bound by the dissipation scale.

We are now going to discuss the slight discrepancies between the two experiments which are basically related to the question of long-term predictability and not to numerics. Figure 5 compares enlargements of the vortex near the stagnation point in both experiments at $t = 10$. As mentioned earlier, the contours almost coincide. They do, up to the accuracy of the plot for the three innermost contours of the vortex core. The outermost contours are engaged in the stripping process. They are apparently less numerous in the contour surgery experiment (where only two are visible) than in the pseudo-spectral counterpart, where one can count five. The reason is that, in the inviscid limit, stripping removes almost completely the outermost vorticity levels from the vortex [13]. Consequently, vorticity levels tend to pile on a single contour on the core boundary. Contour surgery is perfectly able to represent this inviscid process and five contours have merged on the core boundary in Fig. 5b. The innermost of the five separates and becomes visible on the internal side of the expelled filament. On the contrary, the pseudo-spectral method is bound by its dissipation scale and piling, like that seen in the contour surgery experiment, is impossible. Nevertheless, the high resolution used here allows very steep vorticity gradients to develop on the boundary of the core, and the two boundaries in Figs. 5a and b, as well as the expelled filaments, are in excellent agreement at this stage.

Note that the analyticity of the 2D Euler equations [19] prevents an initially smooth vorticity profile to become discontinuous in finite time. Correspondingly, for piecewise-constant vorticity, the recent proof of contour regularity [18] implies that contours cannot approach faster than super-exponentially [20]. However, this rate of approach means that contours can rapidly become indistinguishable, or that continuous vorticity can become virtually discontinuous.

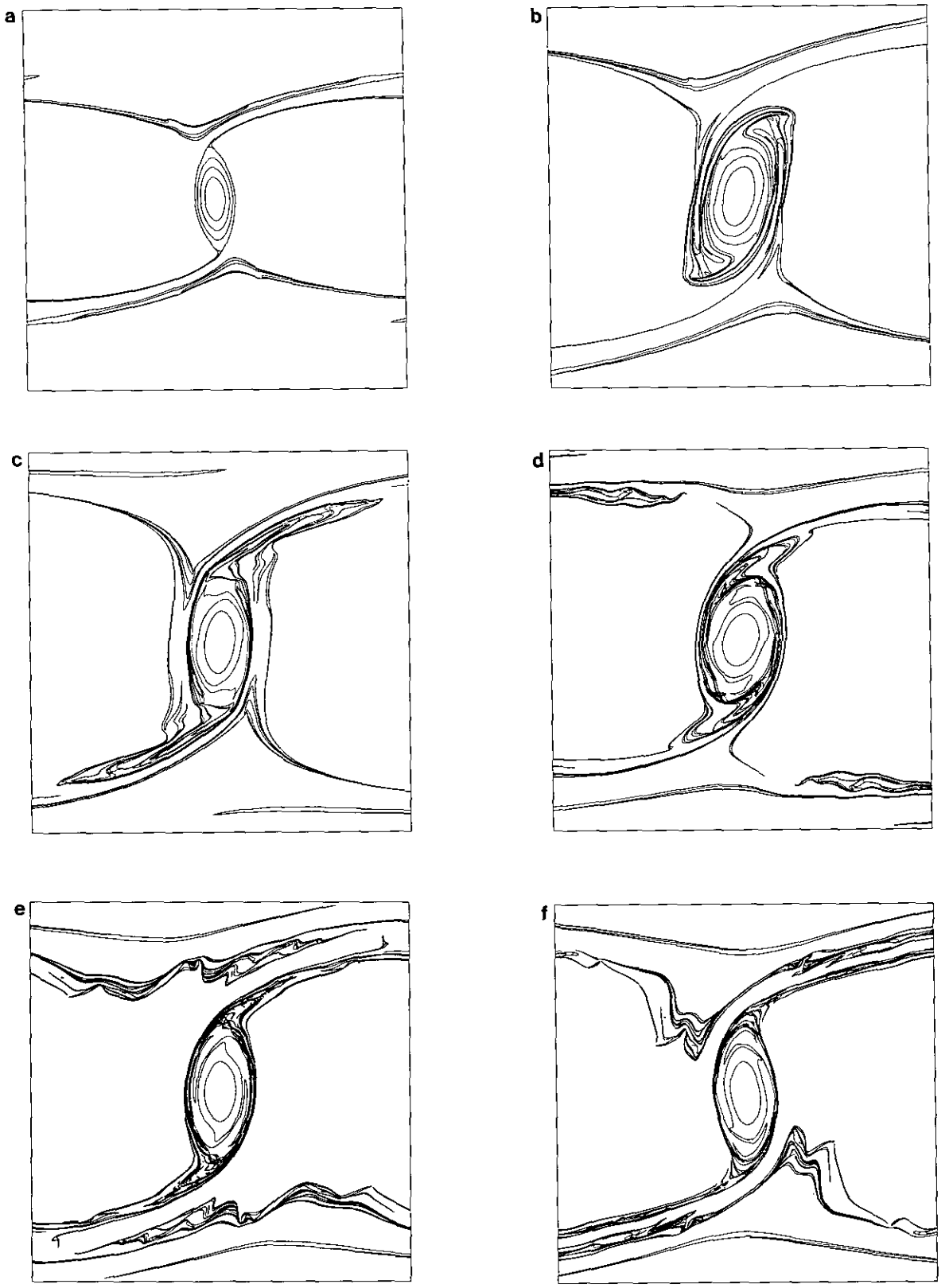

FIG. 4. Vorticity charts taken from the contour surgery experiment using eight-level discretization. The contours are the same as in Fig. 3. The frame of the charts is the full periodic box for (a) and the domain $[-0.6\pi, 0.6\pi] \times [-0.6\pi, 0.6\pi]$ for the other cases: (a) $t = 10$; (b) $t = 15.5$; (c) $t = 17.5$; (d) $t = 21$; (e) $t = 23.5$; (f) $t = 25$.

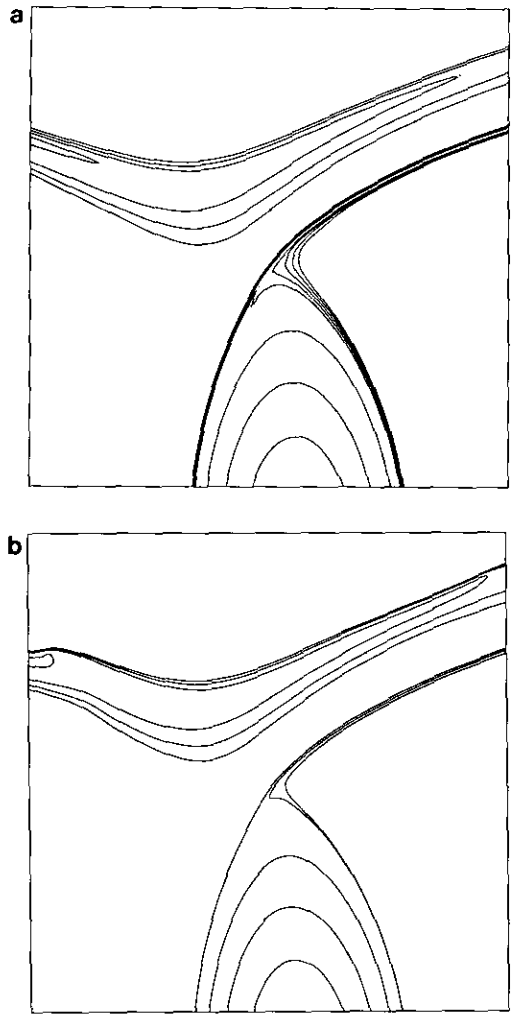

FIG. 5. Enlargement and comparison of the flow at $t = 10$: (a) the pseudo-spectral experiment; (b) the eight-level contour surgery experiment.

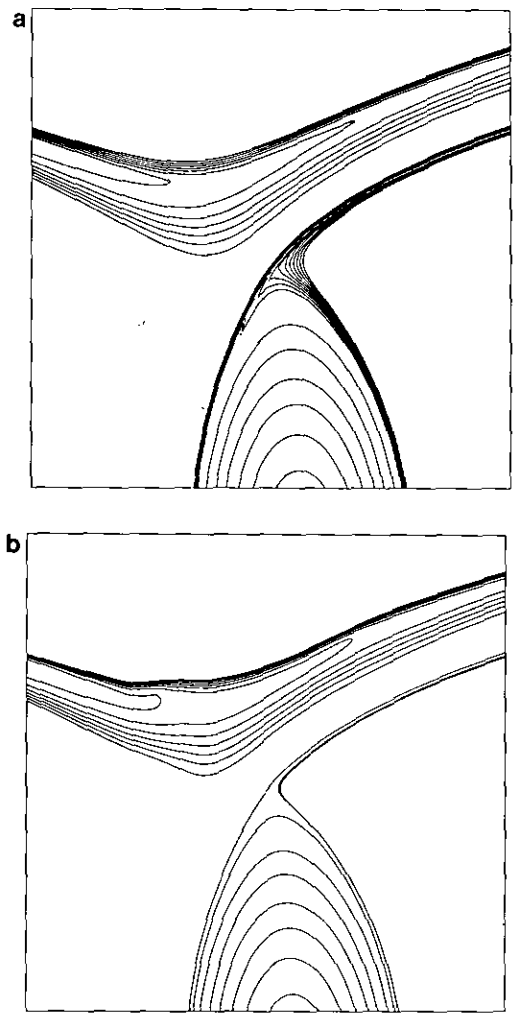

FIG. 6. Same as in Fig. 5 except for the 16-level contour surgery experiment.

The re-entering filament crosses the upper part of the figures. These filaments are essentially passive structures in the flow induced by the combination of the vortex and the shear, but there exists also a slight contribution of the filaments to their own dynamics. This is particularly visible near the tips of filaments in Fig. 5b, where they tend to roll up and induce a kink in the nearby contours. This effect is typical of the dynamics at the extremity of a finite vorticity strip [11] and relies on short-range interactions. This is a consequence of the discretization of the vorticity profile and is not visible in the pseudo-spectral calculation. Figure 6 compares the vorticity distribution calculated by contour surgery with the 16-level discretization and the corresponding chart from the pseudo-spectral case using the same plotting levels. While some effects near the tip of filaments are still visible in Fig. 6b, the slight discrepancies between the two experiments are significantly reduced, compared to Fig. 5.

4.2. *Quantification by Moments*

Detailed inspection of the time sequence partly shown in Figs. 3 and 4 reveals that the shapes of the vortex cores in the two experiments, although very similar, are not identical for $t > 12$. In order to give a quantitative account of the difference, we measured the moments of the vorticity distribution with respect to the center of the vortex. If we denote by D_k the domain enclosed within the vorticity contour $\omega = \omega_k$ (D_k may not be connected), we define the associated moments [6] as

$$\alpha_{mk} = \iint_{D_k} z^{m-1}\, dx\, dy, \qquad m = 1, 2, \ldots, \tag{11}$$

where $z = x + iy$ and x and y are the coordinates with respect to the center of the box. These moments are the coefficients of the Laurent series of the velocity field exterior to

D_k. In this form, they are easily estimated by a summation on the collocation grid in the physical domain. In the contour surgery code, the equivalent contour representation is used,

$$\alpha_{mk} = \frac{i}{2m} \oint_{\mathscr{C}_k} z^m \, dz^*, \tag{12}$$

where $\mathscr{C}_k$ is the bounding contour (or contours) of D_k and * denotes complex conjugation. The first moment α_{1k} is purely real and is in fact the area of the domain D_k. This is theoretically an inviscid constant, owing to material conservation of vorticity and incompressibility. The second moment α_{2k} is proportional to the centroid of D_k and is automatically zero by definition. The third and higher moments correspond to elliptical and higher-order deformations of the region D_k. The twofold symmetry of the experimental problem further implies that all of the even-ordered moments are zero (this symmetry was not imposed in the contour surgery calculation, yet the computed flow remains very nearly symmetric).

We have selected a few internal contours to present the quantitative comparison. These contours do not get stripped from the vortex though they undergo severe deformation, exciting many of the moments. In the case of eight contours, the second and third innermost contours have been selected (hereafter denoted 2:8 and 3:8), and for 16 contours, the fourth, the fifth, and the sixth have been selected (4:16, 5:16, and 6:16). These five contours are nested following the relation $2{:}8 \subset 4{:}16 \subset 5{:}16 \subset 3{:}8 \subset 6{:}16$, see Table I.

Figure 7 compares the variation of the area of the five contours in the two experiments. Each curve shows the area

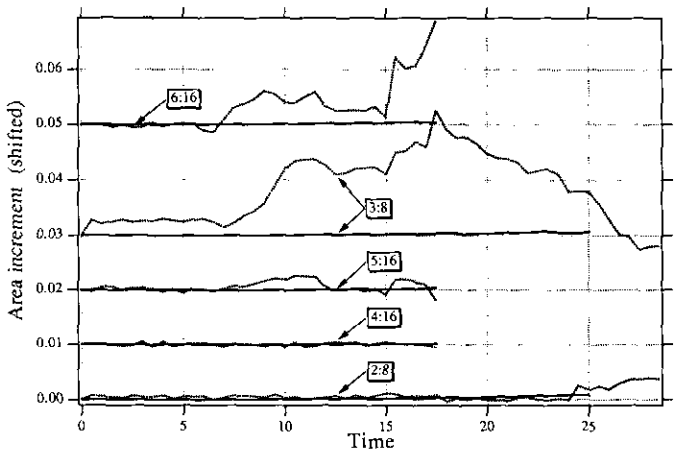

FIG. 7. Area increment, $A(t) - A(0)$, for the five contour levels compared in the two experiments. The solid curves show the results of the eight- and 16-level contour surgery calculations, and the dashed curves show the results of the pseudo-spectral calculation. The curves are shifted by multiples of 0.01 to ease visibility. The initial areas $A(0)$ are $A_{2:8} = 0.386$, $A_{4:16} = 0.409$, $A_{5:16} = 0.521$, $A_{3:8} = 0.603$, and $A_{6:16} = 0.639$.

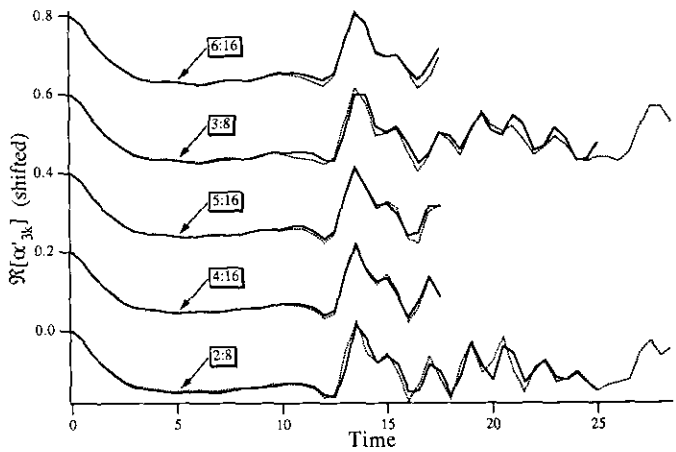

FIG. 8. $\Re[\alpha'_{3k}]$ for the same five contour levels as depicted in Fig. 7. The curves are shifted.

variation of a given contour with respect to its initial area given in the caption. The curves are shifted in the vertical direction to ease comparison. The main result is the excellent conservation achieved by contour surgery over the integration time. The relative variation of the areas of contours 2:8 and 3:8 in the interval $0 < t < 25$ is less than 2.2×10^{-3} and 1.3×10^{-3}, respectively, while the variation for the three 16-level contours is less than 7.8×10^{-4} in the interval $0 < t < 17.5$. In the pseudo-spectral experiment, higher deviations are observed owing to the dissipative flux of vorticity across the contours. The maximum variation is only 3% for the most disturbed contours, 3:8 and 6:16. Much higher variations are observed for the external contours (not shown) which are tracing the dynamics of the filaments. For instance, the area of contour 15:16 undergoes variations of the order of 15%. The better results obtained for contour surgery are due the ability of this method to reach very high effective Reynolds numbers by dynamically refining the resolution at required locations, whereas the pseudo-spectral method is bound by its basic resolution.[1]

Figure 8 shows the variation of the real part of the normalized third-order moment $\alpha'_{3k} \equiv \alpha_{3k}/\alpha_{1k}^2$ for the same five contours as above. Starting from zero, all curves grow in magnitude to a value near -0.15 during the first three units of time. There is a plateau between $t \approx 3$ and $t \approx 11$ that corresponds to the quasi-stationary stage of stripping described above. After $t \approx 11$, a part of each re-entering original arm begins to slide along the edge of the stripped vortex core and interacts strongly with the latter, inducing

[1] Note that the cutoff scale is here larger than the mesh size of the physical domain since a significant number of modes near the truncation scale must be devoted to the dissipation range. More elaborate subgridscale parameterizations, like the *anticipated vorticity* method [15], attempt at suppressing the dissipation range in order to more fully exploit the resolution of the spectral representation.

shape vacillations on it. Figure 8 demonstrates the agreement of both methods over the whole integration. Note also that the curves drawn for the five levels are very close. The reason is that the aspect ratio of the ellipse approximating each vorticity contour is practically constant over the whole vortex core. To our knowledge, this phenomenon has not yet received an appropriate theoretical explanation.

The small discrepancies between the two methods can be attributed to (1) the finite discretization of the profile in contour surgery and (2) the slight dissipation in the pseudo-spectral method. These discrepancies are made more apparent in Fig. 9, where the differences between pairs of curves in Fig. 8 are shown. The differences grow significantly after $t = 12$ when the dynamics becomes more active but they remain bounded. The observed oscillation indicates the principal cause of the differences is a phase shift between the contours in the two calculations. While some of the differences may be attributed to the redistribution of circulation by dissipation in the pseudo-spectral calculation (cf. Fig. 7), the differences are nevertheless reduced significantly, by a factor of three, when twice as many contours are used in the contour surgery experiment.

Higher-order statistics are useful to diagnose non-elliptical deformations. The higher-order moments, however, must be modified to remove the contribution from the dominating elliptical deformation of the vortex. Instead of the moments α_{5k} and α_{7k}, we thus need to consider the cumulants

$$\alpha'_{5k} \equiv \frac{\alpha_{5k}}{\alpha_{1k}^3} - 2\frac{\alpha_{3k}^2}{\alpha_{1k}^4}$$

and

$$\alpha'_{7k} \equiv \frac{\alpha_{7k}}{\alpha_{1k}^4} - 5\frac{\alpha_{3k}^3}{\alpha_{1k}^6}$$

which vanish for an elliptical contour. Figure 10 shows the real part of the differences between the two methods for α'_{5k} and α'_{7k}. The signals remain very small for $t < 11$ when neither α'_{5k} or α'_{7k} are significantly excited. After $t \approx 11$, the vortex core is strongly perturbed and clear non-elliptical vacillations ensue as seen in Fig. 3e. The discrepancies are here more pronounced than for the elliptical component of the deformation with peak values near two standard deviations. Nevertheless, the 16-level discretization shows much reduced differences up to $t \approx 15$. It is remarkable that the improvement of the 16-level discretization over the eight-level discretization is more apparent on Fig. 10 than on Fig. 8. It seems likely that this is due to the fact that low-order deformations can be resolved well with just a few vorticity levels, and one quickly reaches a plateau with increasing numbers of levels. That plateau is not so quickly reached for higher-order deformations. Small-scale Rossby-wave oscillations within discrete levels are simply absent in contour surgery.

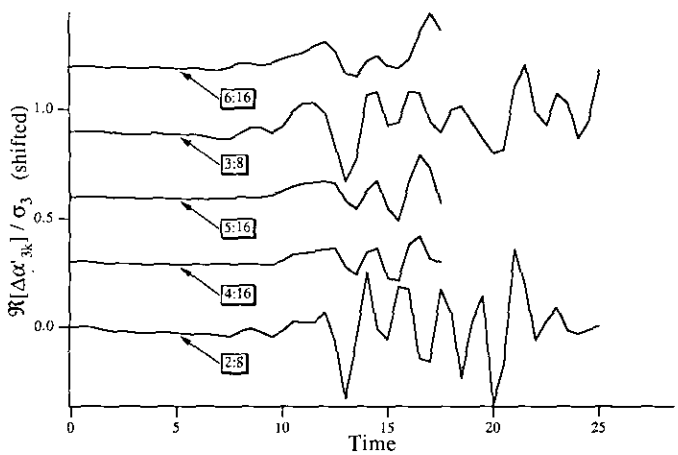

FIG. 9. Normalized differences in $\Re[\alpha'_{3k}]/\sigma_3$ between the two simulation methods for the five contour levels compared, where $\sigma_3 = 0.13$ is the rms deviation of $\Re[\alpha'_{3k}]$ over the five levels. The curves are shifted.

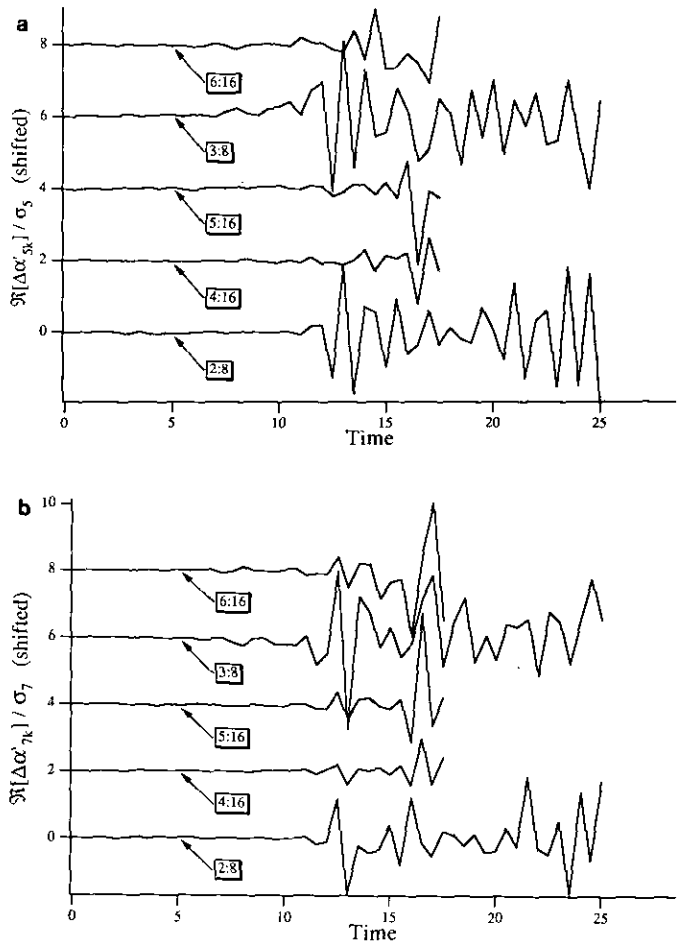

FIG. 10. Normalized differences in (a) $\Re[\alpha'_{5k}]/\sigma_5$ and (b) $\Re[\alpha'_{7k}]/\sigma_7$ between the two simulation methods for the five contour levels compared, where $\sigma_5 = 0.003$ and $\sigma_7 = 0.003$ are the rms deviation of $\Re[\alpha'_{5k}]$ and $\Re[\alpha'_{7k}]$ over the five levels. The curves are shifted.

4.3. *Long-Time Comparison*

Figure 11 shows an enlargement of the vortex at time $t = 17.5$ for the eight-level contour surgery and pseudo-spectral experiments. At this time, the folded re-entering filament has made one and a half rotations around the vortex core and is partly divided again and torn apart by the external shear. Figure 11 shows the complicated structure of the embedded foldings near the stagnation point of the velocity field. As at $t = 10$, the contours pile onto a single curve in the contour surgery experiment while they remain spread out over an observable distance in the pseudo-spectral experiment. This spreading in fact provides a source for further stripping of the vortex since the weak vorticity created at the edge of the vortex core is easily removed by the external shear (at low resolution, this can lead to an undesirably rapid erosion of the vortex [13]). Such stripping would not occur in contour surgery. The streets of small islands in Fig. 11a are due to truncation effects and artifacts of the plotting routine. Several very thin structures which are visible in contour surgery are missing in the pseudo-spectral experiment where they have been dissipated. On the left side of Fig. 11b, one agains see rollup at the filament tip in the contour surgery experiment.

In addition to these details there exists also a larger scale discrepancy seen as a stronger folding of the filaments in the pseudo-spectral experiment than in the contour surgery one near the center and on the right part of Fig. 11b. It is well known that a vacillating elliptical vortex induces chaotic Lagrangian trajectories [17]. This has been demonstrated for periodic oscillations but is a fortiori true for non-periodic ones. The essential ingredients for this chaos are (1) sensitivity of trajectories near the hyperbolic stagnation point and (2) reinjection of material along the separatrices

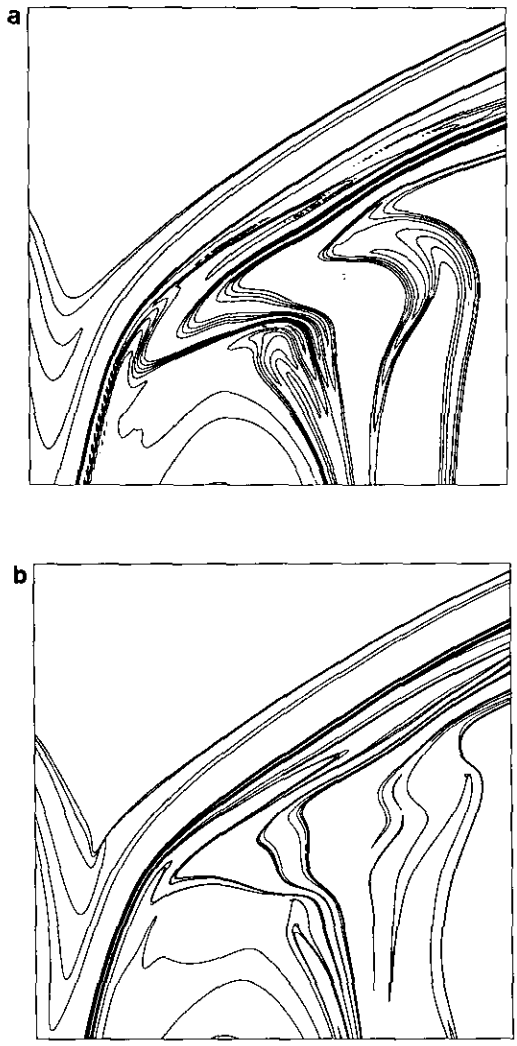

FIG. 11. Enlargement and comparison of the flow at $t = 17.5$: (a) the pseudo-spectral experiment; (b) the eight level contour surgery experiment.

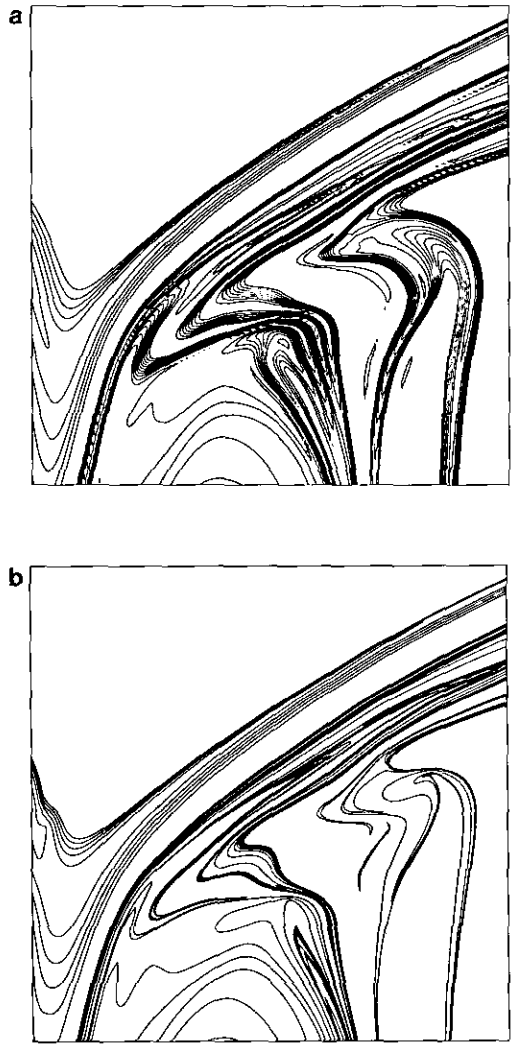

FIG. 12. Same as in Fig. 11 except for the 16-level contour surgery experiment.

of the mean flow. The residence time of a particle near the stagnation point and its exit along one of the two unstable directions can be governed by small amplitude perturbations. It is thus likely that the slight discrepancies due to the discretization of the distributed vorticity profile in contour surgery or the arrested gradient intensification in the pseudo-spectral method are strongly amplified in this region. These discrepancies are nevertheless less noticeable when the resolution of the discrete profile increases, as seen, for instance, in Fig. 12. The effects of contour piling and dissipation of thin structures are still visible here but the agreement between the two experiments has also been significantly improved over that shown in Fig. 11.

At later times, the repeated folding and stretching of filaments generates a cascade to smaller and smaller scale structures around the vortex while the core retains its initial profile. The small scales are smoothed out in the pseudo-spectral simulation. Figures 3h and i show that many details are lost between $t = 21$ and $t = 23.5$ on the periphery of the vortex. In contour surgery, some of these details are removed by surgery, though significantly fewer than in the pseudo-spectral experiment. The price to pay is, however, the introduction of many new points which make the calculation more and more costly as time proceeds. For this reason, only the eight-level discretization is used for $t > 17.5$.

An enlargement at $t = 23.5$ is shown in Fig. 13. It is still remarkable that the two vorticity distributions are in such good agreement in spite of the long integration time. Much greater detail is visible in the contour surgery experiment than in the pseudo-spectral one. See, for instance, the complicated foldings occurring near the stagnation point or the cascade of filamentation near the center of the enlargement

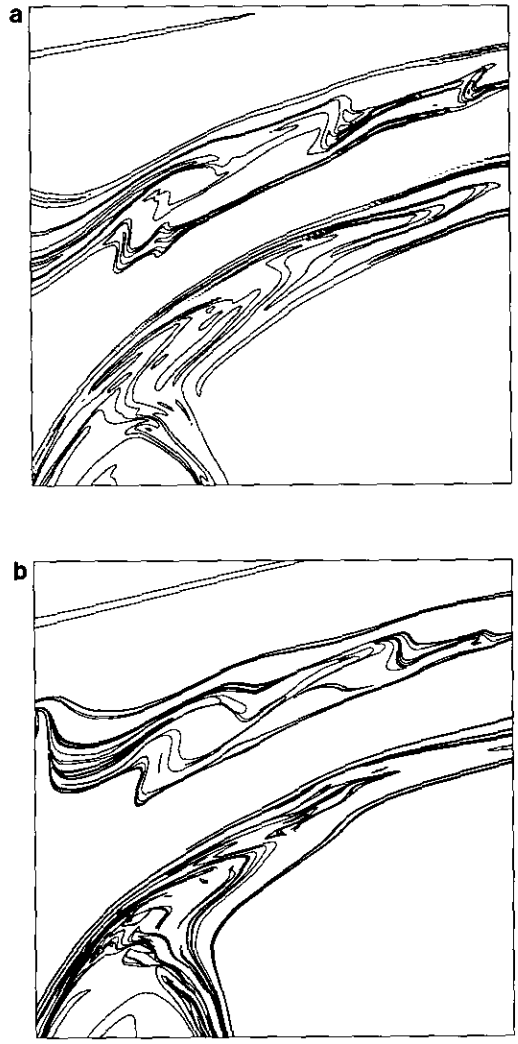

FIG. 13. Enlargement and comparison of the flow at $t = 23.5$: (a) the pseudo-spectral experiment; (b) the eight-level contour surgery experiment.

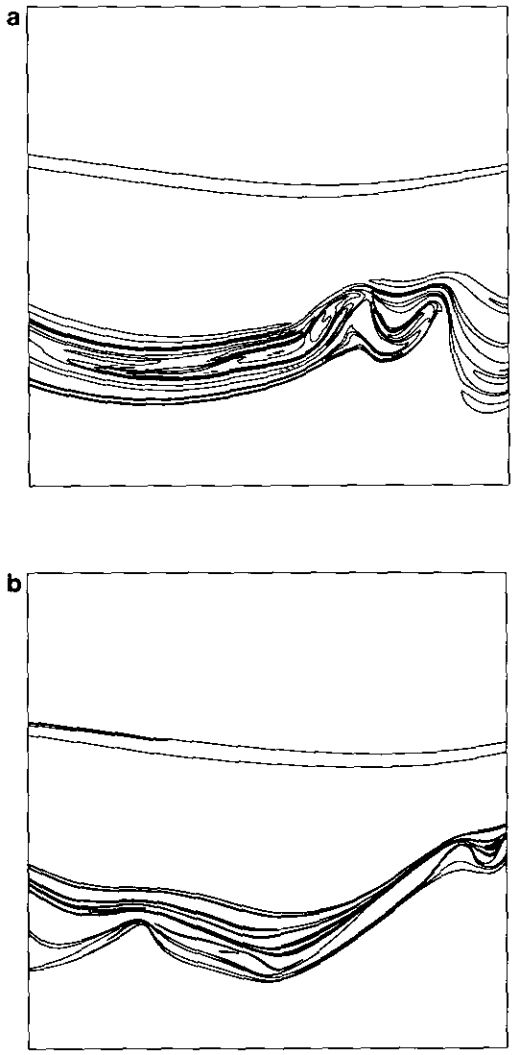

FIG. 14. Further enlargement and comparison at $t = 23.5$.

in Fig. 13b, both of which are absent in Fig. 13a. The most noticeable discrepancies are visible on the re-entering filaments which are enlarged in Fig. 14. The different locations and amplitudes of the folds can be traced back to the passage of the filaments near the stagnation point. They are the consequence of the sensitive dynamics described above. As a consequence, the approach of the vortex by the re-entering filaments occurs differently at $t = 25$ in the two experiments. In Fig. 3j, a single fold develops on the incident side of the vortex and a complicated folded structure is seen above and below the stagnation point, while in Fig. 4f two folds are formed on the incident side and the folded structure has already been torn apart. It is clear that these effects lead to stronger and stronger differences at later times. It is also clear that the essence of these differences is not numerical but rather the chaotic nature of the dynamics which implies exponential amplification of small perturbations.

5. DISCUSSION

The main result of this article is the mutual validation of the pseudo-spectral and contour surgery algorithms in an experiment involving the stripping of a distributed vortex with subsequent complex interactions between the vortex core and the stripped filaments. In contour surgery, a continuous profile of vorticity has to be discretized with a finite and small number of steps (here, 8 or 16). Nevertheless, no significant spurious dynamical behaviour is observed in the contour surgery experiment. On the contrary an excellent quantitative agreement is obtained between the two types of simulation, up to very small scales of motion.

The small differences are due to the ability of contour surgery to resolve much smaller scales than the pseudo-spectral method. Contour surgery can describe sharpening of vortex edges by stripping and the cascade of filamentation several ranges of scales beyond what can be done with the pseudo-spectral method. The resolution used here in the pseudo-spectral calculation is close to the state-of-the-art limit for this kind of study.

The discretization of vorticity within contour surgery is not without its side effects. The first is the overly dynamical behavior of the tips of filaments, seen in Fig. 5b, for example. Here, the discrete nature of the vorticity field is most noticeable. A second is the slight inaccuracy in representing waves on the contours within the vortex core. Both effects are reduced substantially by doubling the number of contours used, indicating rapid convergence to the theoretical continuum behavior.

This convergence is more rapid than indicated by the seemingly coarse representation of the vorticity. The essential point is that the representation of the velocity is far better; the difference between the velocity field corresponding to a continuous distribution of vorticity and one corresponding to a discretization of this distribution into N levels scales as $1/N^2$, indicating a *quadratic* convergence to the continuum behaviour. It is the velocity field, after all, which is responsible for the evolution of the vorticity distribution.

A corollary based on additional comparisons not shown here is the surprising lack of sensitivity of the complicated dynamical processes investigated in this paper to the detailed profile of the vortex, provided essential invariants are the same. This is another illustration of the domination of large scales in two-dimensional flows.

We do not intend to say that one method is superior to the other in all circumstances. The pseudo-spectral method is a general purpose algorithm which has been widely used in turbulence studies, where there exist many vortices and appreciable vorticity between the vortices, in particular for strong forcing [9]. In this case, uniform resolution may be a desirable property when it is difficult, if not impossible, to encompass a flow within a hierarchy of structures. Contour surgery, on the contrary, is suited to practically inviscid, unforced, vortex-dominated flows, wherein sharp vorticity gradients are commonplace and localized vortices control essentially the entire flow evolution. Processes like filamentation [4, 5] and stripping [13], which involve a wide range of spatial scales, can be handled efficiently, and contour surgery is ideal for the study of simple vortex interactions [8, 7]. Moreover, with the recent development of "moment-accelerated contour surgery" [6], it is now possible to cope with a large number of structures and thus to investigate some of the mechanisms of 2D turbulence at much higher Reynolds numbers than those accessible to the pseudo-spectral method.

ACKNOWLEDGMENTS

The computer resources were allocated by the Scientific Council of the Centre de Calcul Vectoriel pour la Recherche and by the Manchester Computer Centre through a grant from the Science and Engineering Research Council. Several figures were plotted using the NCAR graphics software.

REFERENCES

1. D. Gottlieb and S. A. Orszag, *Numerical Analysis of Spectral Methods: Theory and Applications* (SIAM, Philadelphia, 1977).
2. A. Leonard, *J. Comput. Phys.* **37**, 289 (1980).
3. N. J. Zabusky, M. H. Hughes and K. V. Roberts, *J. Comput. Phys.* **30**, 96 (1979).
4. D. G. Dritschel, *J. Fluid Mech.* **194**, 511 (1988).
5. D. G. Dritschel, *Comput. Phys. Rep.* **10**, 77 (1989).
6. D. G. Dritschel, *Phys. Fluids A* **4**, 1737 (1992).
7. D. G. Dritschel and D. W. Waugh, *Phys. Fluids A* **4**, 1737 (1992).
8. D. W. Waugh, *Phys. Fluids A* **4**, 1745 (1992).

9. B. Legras, P. Santangelo, and R. Benzi, *Europhys. Lett.* **5**, 37 (1988).
10. T. F. Buttke, *Phys. Fluids A* **1**, 1283 (1990).
11. D. G. Dritschel and M. E. McIntyre, *Phys. Fluids A* **2**, 148 (1990).
12. D. G. Dritschel and N. J. Zabusky, *J. Comput. Phys.* **93**, 481 (1991).
13. D. G. Dritschel and B. Legras, *Phys. Fluids A*, submitted.
14. C. Basdevant, *J. Comput. Phys.* **50**, 209 (1983).
15. R. Sadourny and C. Basdevant, *J. Atmos. Sci.* **42**, 1353 (1985).
16. J. M. Ottino, *The Kinematics of Mixing: Stretching, Chaos and Transport* (Cambridge Univ. Press, Cambridge, UK, 1989).
17. L. M. Polvani and J. Wisdom, *Phys. Fluids A* **2**, 1283 (1990).
18. J.-Y. Chemin, *C. R. Acad. Sci. Paris Ser. I* **312**, 803 (1991).
19. W. Wolibner, *Math. Z.* **37**, 668 (1933).
20. A. L. Bertozzi and P. Constantin, Global regularity for vortex patches, preprint.